Department of Metallurgy & Materials Science

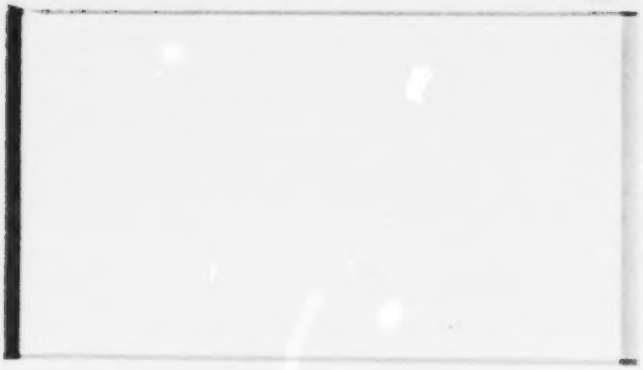

University of Toronto

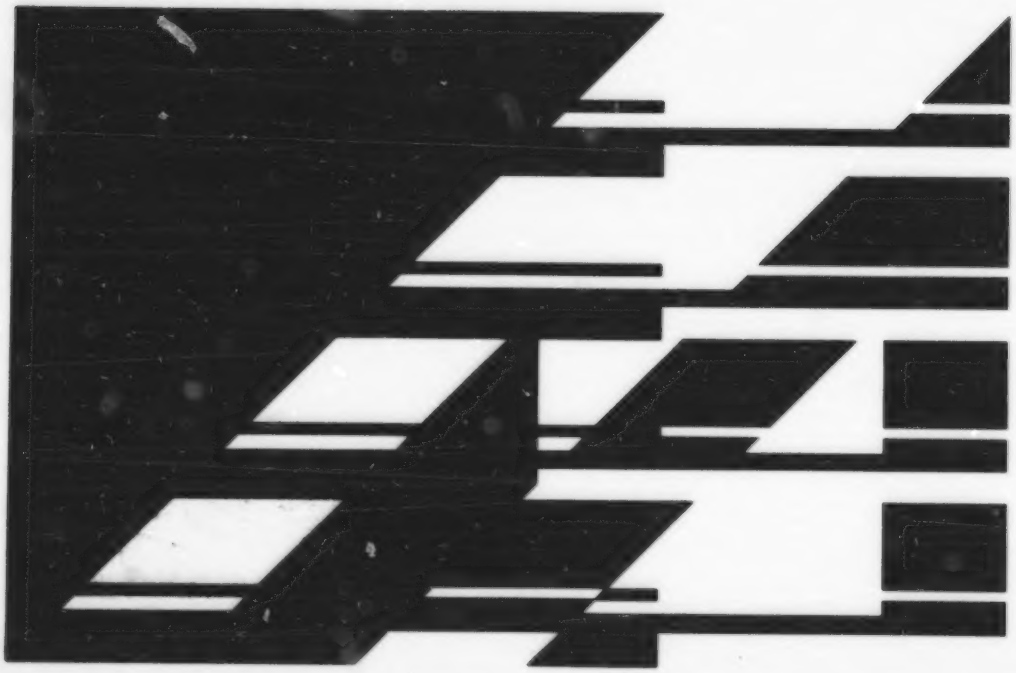

Characterization of Precipitates in the Weld HAZ for a Range of Offshore Steels

G.C. Weatherly, Zhi-Min Yin and M. Wolosiuk
Department of Metallurgy and Materials Science
University of Toronto
Toronto, Canada M5S 1A4

CONTRACT REPORT NUMBER OST85-00255
CONTRACTOR: University of Toronto
REQUISITION NUMBER 23440-5-9173

Final report prepared for the Department of Energy, Mines and Resources, P.M.R.L. (CANMET), 568 Booth Street, Ottawa K1A 0G1 under D.S.S. Contract 20ST. 23440-5-9173.

45 pp

MICROMEDIA

Abstract

A detailed study was made of the dissolution, precipitation and compositional changes associated with microalloying elements (Nb, V, Ti) in a series of HSLA steels. Both welds and Gleeble simulated samples were studied and compared at two heat inputs, 3 and 6 kJ/mm, for 4 steels, BS4360 and LT60 which are Nb and Nb-V grades, and 350 WT CAB and 350 WT STRAND, which are Nb-V-Ti containing steels. The behaviour of the Nb and Nb-V grades was dictated by the dissolution behaviour of the coarse Nb-rich particles found in the base plate of both steels. The Gleeble samples of the BS4360 steel showed nearly complete dissolution of the particles, in reasonable agreement with the predictions of a model based on diffusion controlled dissolution. The LT60 steel contained a coarser size distribution of Nb carbo-nitrides; this, coupled with the greater microalloying content of this steel resulted in a greater fraction of particles surviving the weld cycles in LT60 than BS4360. Reprecipitation effects were observed in the LT60 welds at the higher heat input but not in the Gleeble simulated samples.

The Ti-Nb bearing steels showed more complex behaviour than the Nb, V-containing steels because the particle composition was dependent on the history of the steel and the particular thermal cycle. In general, the mean Ti/Nb content of the particles increased after Gleeble thermal cycling and as the fusion line was approached in the actual welds. The increase was attributed to the loss of Nb caps and the formation of Ti-rich skins at the cuboidal particles. In the Gleeble samples all the fine spheroidal particles dissolved after the thermal cycles, but again in the welds reprecipitation effects were observed. The difference in behaviour of the welds and Gleeble samples at the same nominal heat input was attributed to the slower cooling rates in the bay region of the welds and the possible role of deformation in the HAZ of the weld promoting precipitation on cooling.

The transformation products produced on cooling the Gleeble samples were studied by S.E.M. and T.E.M. techniques. The formation of ferrite or bainite structures and the appearance of MA or carbides in the inter-ferrite regions was shown to be related to the C content and cooling rate of the weld. The MA phase was favoured at low C levels (at a fixed heat input) and faster cooling rates (lower heat inputs) for a given steel.

List of Contents

		Page No.
	Introduction	4
PART A	**PRECIPITATE CHARACTERIZATION**	5
1.	**B.S. 4360-D**	
1.1	Preparation of Replicas	5
1.2	E.D.X. analysis	6
1.3	Base metal microstructure	6
1.4	3 and 6 kJ/mm Gleeble samples	9
1.5	3 kJ/mm Weld	10
2	**LT60**	
2.1	Base Metal microstructure	10
2.2	3 and 6 kJ/mm Gleeble samples	10
2.3	3 and 6 kJ/mm Welds	11
3	**350WT CAB**	
3.1	Base metal microstructure	11
3.2	3 and 6 kJ/mm Gleeble samples	12
3.3	3 and 6 kJ/mm Welds	12
4	**350 WT STRAND CAST**	
4.1	Base metal microstructure	13
4.2	3 and 6 kJ/mm Gleeble samples	13
4.3	3 and 6 kJ/mm Welds	15
5	**References**	
	Figures for PART A	16-31
PART B	**CHARACTERIZATION AND IDENTIFICATION OF MICROSTRUCTURAL TRANSFORMATION PRODUCTS**	32
	Figures for PART B	36-42
PART C	**CONCLUSIONS**	43-44

Introduction

This report deals with the results of a study of the characterization of precipitates and the microstructure in the weld heat affected zone of four candidate steels being considered for offshore construction applications. The work statement as supplied in Appendix A of the contract requested that the following tasks be performed:

1. Prepare extraction replicas taken from the bay region of the HAZ to include up to a distance of 2mm from the fusion line for bead on plate welds produced at heat inputs of 3 and 6 kJ/mm for the following four steel grades:

   a) BS4360D
   b) LT60
   c) 350WT (CAB treated)
   d) 350 WT (Strand Cast)

2. Prepare extraction replicas and thin foils from 3 and 6 kJ/mm simulated samples for the above four steels.

3. Characterize the precipitates present in the extraction replicas using energy dispersive x-ray microanalysis. In the case of the replicas taken from the bay region of the weld precipitate location with respect to the fusion line should be established.

4. Examine thin foils in the TEM to identify microstructural constituents present and if possible locate high and low angle boundaries in relation to this microstructure.

The composition of the four steels is given in Table I below.

Table I - Composition of Four Steels

Steel	C	Mn	Si	Ni	Cr	Mo	V	Nb	Ti	N(ppm)
BS4360D	.14	1.33	.37	.01	.015	.01	-	.027	-	73
LT60	.12	1.29	.272	.135	.151	.01	.053	.039	-	70
350WT(CAB)	.15	1.44	.24	.255	.04	-	.06	.02	.01	72
350 WT(STRAND)	.07	1.35	.286	.255	.24	.01	.068	.022	.01	62

BS 4360D and LT60 are ingot cast products which after rolling had been normalized . 350WT Strand Cast had been reheated to 1175°C, controlled rolled with a finishing temperature above 755°C and stack

cooled below 400°C. 350WT CAB treated steel has essentially the same microalloying content as the strand cast steel, but was ingot cast before being subjected to the same rolling practice as the continuously cast steel. Although the contract called for actual weld and Gleeble simulated samples to be studied at heat inputs of 3 and 6 kJ/mm for all steels, shortage of material for the BS4360D steel restricted the welding study to a heat input of 3kJ/mm.

The experimental procedure, results and discussion are divided into two parts in the report. In part A, the results of the precipitate characterization for each of the four steels are considered separately; in part B, the results of the characterization and identification of the microstructural transformation products are summarized.

Part A Precipitate Characterization

1. BS4360-D

1.1 Preparation of replicas

The method of preparation of the replicas from the bay region of the weld is described in some detail in this section. Identical procedures were followed for all weld samples.

A mounted section from the relevant portion of the weld was prepared by standard metallographic techniques and etched for 5-10 secs in a solution of 3% nital. The bay region of the weld could then be readily identified. A thin carbon coating (~ 20-30nm thick) was then deposited onto the etched surface and subsequently scored into sections ~ 2½ x 2 mm in area.

The scoring was done so that in the bay region of the weld, the replica would span both the weld metal and the heat affected zone region up to 2mm from the fusion line. A protective lacquer coating was then applied to the sample so that all areas of the C film except the region of interest (the bay region) would be protected during electrolytic stripping of the film. This was done by electropolishing in an electrolyte of 16% perchloric acid, 64% ethanol, 9% butylcellusolve and 11% distilled water. When successful the end result was a rectangular C film (2 x 2½mm), the short side of which lay nearly parallel to the fusion line, with the long side running into the heat affected zone. The weld metal could be readily identified by the presence of oxide inclusions (Fig. 1a), the fusion line by an area devoid of precipitates (Fig. 1b) and areas into the heat affected zone by traversing the sample in the appropriate direction away from the fusion line (Fig. 1c).

In order to complete the characterization of the precipitates, extraction replicas were also prepared from the base metal at a point remote from the HAZ where the structure would have been unaffected by the weld thermal cycle. Replicas were also taken from the Gleeble samples, using the central area of a cross-section prepared from the mid-line of the thermally cycled specimens which experiences the maximum temperature during the simulated thermal cycle.

1.2 EDX analysis

Energy Dispersive X-ray analysis (EDX) was used to determine the chemical composition of the precipitates. These particles were sufficiently thin that the Cliff-Lorimer k factor approach [1] could be used directly to determine their composition. For the BS4360D steel, the k-factor approach was not necessary as the particles of interest contained only Nb (in addition to C and N). For the other three steels, the k factors previously determined for this class of HSLA steel were adopted [2,3].

1.3 Base metal microstructure

The precipitates in the base plate of the 4360 steel had a bimodal size distribution - a coarse fraction 50-300 nm in size, and a much finer fraction 5-15 nm in diameter (Fig. 2). Both sets of particles contained Nb. The coarser fraction presumably form during hot rolling and are stable at the maximum temperature used during the normalizing heat treatment; the fine particles probably represent that fraction of the total Nb(C,N) constituent that is soluble at the normalizing temperature and precipitate out during air cooling. The size distribution of the coarser particles is shown in Fig. 3. Approximately 150 particles were measured to arrive at this size distribution, which involved sampling about 40 different areas of a 600 mesh grid sample, each area of which contained only 3 to 5 large particles. (This point is made to emphasize some of the difficulties that are encountered in obtaining statistically significant data from the weld samples - see below).

1.4 3 and 6 kJ/mm Gleeble samples

The thermal cycles for the 3 and 6 kJ/mm Gleeble samples were determined at P.M.R.L., CANMET and are reproduced in Table II. From the

Table II Thermal Cycles for Gleeble Experiments

3kJ/mm Thermal Cycle

Total Elapsed Time	Pyrometer Temp.(°C)	Thermocouple Temp.(°C)
3.38S	1350	1350
3.49S	1376	1376
3.69S	1376	1376
4.09S	1365	1365
4.49S	1300	1319
8.09S	985	1078
11.69S	787	900
13.69S	695	807
16.89S	605	709

$\Delta t_{800\text{-}500°C}$ = 20s

6 kJ/mm Thermal Cycle

3.38S	1350
3.49S	1375
3.99S	1375
4.39S	1365
4.79S	1300
6.99S	1200
15.99S	1000
29.99S	800
59.99S	700

$\Delta t_{800\text{-}500°C}$ = 68s

data in this table we note that the heating rate and time at peak temperature are similar for the two heat inputs but the cooling rate for the higher heat input is much slower ($\Delta t_{1375\text{-}1000°C}$ ~ 4.4s at 3kJ/mm compared to ~12s at 6kJ/mm).

After both thermal cycles, almost all the large and all of the fine

particles had dissolved. In the majority of the grid areas examined, no Nb-containing particles were detected; the maximum size of particles observed to contain Nb was ~ 100 nm and these particles were confined to a few isolated locations of the replica. From this observation it appears that all the particles < 200 nm in diameter in the starting microstructure (Fig. 3) have dissolved during the thermal cycles.

The rate of dissolution of particles during weld thermal cycles can be calculated following the procedures described by Suzuki et al.[4]. Fig. 4 shows the results of a calculation using the thermal cycles of Table II for a steel containing 0.027 wt % Nb and 0.14 wt % C. The equilibrium solubility temperature of NbC for this steel, correcting for the Mn, Si and Cr content as described by Sharma et al. [5] is approximately 1100°C. The size range of particles that dissolve during a thermal cycle is determined by the time spent above this temperature. The points of dissolution of different particle sizes is marked on the two thermal cycles shown on Fig. 4. The max^{m} size of particles that dissolve during the 3kJ/mm thermal cycle is predicted to be ~ 120nm while in the 6 kJ/mm cycle, the max^{m} size is ~ 140 nm. The experimental observations show that the theory slightly underestimates the actual rate of dissolution. The possible reasons for this discrepancy are best considered by referring to the approximate expression for the dissolution time given by Aaron and Kotler[6]. Under isothermal conditions the dissolution time of a spherical particle of radius R_o in a dilute alloy is

$$t_H \doteq \frac{R_0^2}{/k/D_v} \qquad (1)$$

where $/k/ = 2(C_1-C_H)/(C_p-C_1)$ and D_v is the volume diffusion coefficient of the rate controlling species e.g. $D_{Nb/\gamma}$ in the present case. C_1, C_H and C_p are respectively the solute concentration in the matrix at the precipitate-matrix interface, the far field composition and the composition of the precipitate. For the Nb levels of interest in this study, $C_p >> C_1 >> C_H$ and $C_p = 0.5$ (assuming the particles are NbC), so that

$$t_H \doteq \frac{R_0^2}{4C_1D_v} \qquad (2)$$

C_1 is assumed to be given by the solubility product for NbC [5], and D_v is taken from the study of Sparke et al.[7].

Under non-isothermal conditions an approximate expression for the size of the particles that would dissolve at any point in the thermal cycle is given by

$$R_0^2 = \sum_i 4(C_I D_V \Delta t)_i \qquad (3)$$

In equation (3) the thermal cycle is divided into a series of steps of duration Δt_i, in each of which the interface concentration $(C_I)_i$ and diffusion coefficient $(D_V)_i$ are assumed constant. This expression can be used in place of the more rigorous description given by Suzuki et al. [4], but leads to similar numerical results. In the present case the product $\Sigma_i C_I D_V$ summed over the critical temperature range for dissolution, 1100-1375°C, would need to be about a factor of 3 x greater than the assumed values to bring the experimental times and calculated times for dissolution into better agreement. In light of the uncertainty in any diffusion measurement and the scatter in the reported solubility data for NbC[8], we conclude that the experimental and theoretical results are in reasonable agreement, given this uncertainty in the available data.

1.5 3kJ/mm weld

The distribution of particles in the HAZ bay region of the 3kJ/mm weldments was determined by following the procedures described above. The results are shown in Fig. 5 which plots the size of any Nb-containing particle detected as a function of distance from the fusion line for a single replica. Given the low density of coarser NbC particles detected in the base plate (~3-5/grid area), the statistical significance of the data shown in Fig. 5 is not high. Nevertheless the trend seems clear. A region ~ 0.15 mm in width adjacent to the fusion line contained no particles; the mean size of particles then increased from ~ 60 nm to ~ 140 nm out to 1 mm from the fusion line and thereafter there was little further change in the mean particle size to 2 mm. Throughout the area examined all the small particles have dissolved.

When this result is compared to the 3 kJ/mm Gleeble simulation results described earlier it appears that a peak temperature of 1375°C occurs in a distance < 0.3mm of the fusion line in the actual weld. (This comparison assumes that the thermal cycles of Gleeble sample and the weld are similar - in practise the bay reigon should experience a slower cooling rate, so that the estimate of a distance < 0.3mm for a peak

temperature of 1375°C is a conservative one, and should represent the upper limit.)

2. LT60

2.1 Base metal microstructure

The microstructure of the LT60 steel was similar to that of BS4350D, which would be expected from their similar chemistries, and the fact that both steels were in the normalized condition. A bimodal distribution of particle sizes was observed (Figs 6,7). The coarse particles contained only Nb (Fig. 6b), while the fine particles were Nb rich, but also contained V (Fig. 6c). The coarser size distribution ranged from a mimimum of 125nm to a maximum of 650nm, with a mean diameter of 300 nm. (Fig. 7)

2.2 3 and 6 kJ/mm Gleeble samples

The two Gleeble samples gave essentially identical results. All the fine particles had dissolved for both thermal cycles and the mean size of the coarser particles had decreased after the thermal cycle. Fig. 8 shows the size distribution after the 6 kJ/mm thermal cycle; the particles range in size from 100 to 400 nm in diameter with a mean size of 270 nm. The obvious difference in the behaviour of the LT60 and BS 4360D steels after thermal cycling can be related to the size distribution in the two steels. Particles up to 650 nm in size and a mean particle size of 300 nm in the base plate of the LT60 steel are both double the corresponding numbers for the BS4360D steel, so that many more particles will survive the same thermal cycles in LT60, as observed.

2.3 3 and 6 kJ/mm Welds

The distribution of particle sizes in the heat affected zone as a function of the distance from the fusion line is shown in Fig. 9. Again we note the difficulty in obtaining statistically significant trends with this data because of the low density of coarse particles/grid area in the extraction replica of the base plate (3-6 particles/area). A region ~ 0.15 mm in width adjacent to the fusion line in both welds contained no coarse particles. The dissolution behaviour of these particles and the trends shown in Fig. 9 are expected in light of the results of the 3 and 6 kJ/mm Gleeble samples.

There was one significant difference observed between the weld and Gleeble sample for the higher heat input. In the Gleeble sample no fine scale precipitation was observed, but in the weld extensive precipitation was found throughout the HAZ (Fig. 10). This precipitation must occur

during the coating cycle of the weld [4]. Two factors could account for the differences observed between the Gleeble sample and the actual weld at 6 kJ/mm. Firstly, the cooling rate in the bay region of the weld will be slower than that in the Gleeble specimen, so that there will be more time for precipitation effects to occur in the weld. Secondly, the residual stresses in the weld will be higher so that there will be more extensive plastic flow in the austenite region in the HAZ of the weld than in the Gleeble sample. Since the precipitation kinetics of carbo-nitride particles is dependent upon prior deformation [9], this factor should also favour precipitation during cooling in the weld.

3. 350WT CAB

3.1 Base metal microstructure

The base plate contained a mixture of coarse (50-450 nm) and fine (< 20 nm) particles (Fig. 11). Many of the coarse particles were duplex in nature, containing spheroidal Nb-rich caps on a Ti-rich cuboidal core [2,3]. Examples of this behaviour can be seen in Fig. 11. The size distribution of the coarse particles was determined by measurement of ~ 150 particles from extraction replicas. The particles ranged in size from 50-450 nm with a mean diameter of 150 nm (Fig. 12). The average composition of the coarse particles (i.e. accounting for both the core and the cap by using a defocussed electron beam) was measured by EDX analysis using a Cliff-Lorimer k factor of 0.52 for the Ti-K_α and Nb-L radiation [2,3]. This gave an average value of Ti/Nb (expressed as a weight ratio) of 1.94 ± 0.57 (based on 35 readings) with maximum and minimum readings of 3.06 and 0.81. The small particles contained Nb and V with lesser amounts of Ti, but no attempt was made in this study to quantify the mean composition of these small particles.

3.2 3 and 6 kJ/mm Gleeble samples

After Gleeble thermal cycling all of the small particles had dissolved while the coarser particles had lost their "caps" and had a more faceted morphology (Fig. 13). The size distribution of these coarse particles is shown in Fig. 14 after thermal cycles of 3 and 6 kJ/mm. The distributions are similar to those in the base plate although a few of the coarser particles in the starting distribution have partially dissolved. The Ti/Nb ratio in the particles increased from 1.94 ± 0.57 in the base plate to 2.50 ± 0.97 after 3 kJ/mm. This change can be attributed to the loss of the Nb-rich caps on the cuboids and the formation of Ti-rich outer layers on the cuboids, both of which were also observed in a previous study of

particles in welds in Nb-Ti bearing HSLA steels [2,3].

3.3 3 and 6 kJ/mm Welds

The size range and composition of the coarse particles (discussed in sections 3.1 and 3.2 above) in the bay area of the HAZ of the welds were determined by following the same procedures, as described for the BS 4360D and LT60 steels. Again the relatively low density of particles extracted on the replicas made any statistical anlaysis of the mean size of the particles as a function of distance from the fusion line a meaningless exercise. Between 5 and 10 particles were found on any one grid area and given the scatter in the size of these particles no trends could be detected. However, the composition of these particles did show a significant variation as the fusion line was appraoched. This trend is shown in Fig. 15 for the 3 kJ/mm weld (note again that no coarse particles were detected in a 0.1 mm wide zone adjacent to the fusion line). A similar explanation as was advanced to explain the trends in the Gleeble samples can be used to interpret these results. The 6 kJ/mm weld results showed a similar behaviour.

Fine scale (5-20 nm) precipitation was observed throughut the HAZ region at both heat inputs (Fig.16). Again we note that the Gleeble samples of the same steel showed no evidence of reprecipitation, so that these small precipitates must form in the bay region of the weld during the cooling leg of the thermal cycle after dissolution at or near the peak temperature.

The explanation of this effect follows the reasoning given in Section 2.3 for the LT60 steel. The total (V + Nb) content of the 350 WT CAB steel is .08 wt % compared to .092 wt % in LT60, while the C level in the 350 WT CAB steel is slightly higher (0.15 wt % vs 0.12 wt %). The start temperature/time for precipitation of (Nb,V)(C,N) particles during cooling should be similar for those two steels, so the similarity in this behaviour is not unexpected.

4. 350 WT STRAND CAST

4.1 Base metal microstructure

The base plate microstructure of this steel contained a wide range of particle morphologies of variable composition. Fig. 17 illustrates the different particle morphologies found, viz. cuboidal, rounded cuboidal, spheroidal (Fig. 17a) and faceted star-shaped particles (Fig. 17b). The coarser particles in the structure were usually faceted or rounded cuboids, while the finer particles were spheroidal. The star-shaped particles are believed to be formed by the in-situ transformation of dendritic Nb-rich carbo-nitride particles (produced in the as-cast structure) during

reheating and controlled rolling [2,3].

The size distribution of the particles > 25 nm in diameter is shown in Fig. 18. The mean size, 77 nm, is significantly smaller than the other three steels of this study; in particular it is interesting to note that the 350 WT STRAND CAST steel which is made by continuous casting has a much smaller particle size than the 350 WT CAB steel treated steel, which is ingot cast, althugh both steels have the same V, Nb, Ti and N contents. The average Ti:Nb ratio in these particles (following the procedure described for the 350 WT CAB steel) was determined to be 0.90 ± 0.31 with minimum and maximum values of 0.25 and 2.10. Expressing the data in this way is rather misleading, however, as the smaller particles are richer in Nb than the larger particles. For example in the size range from 25 to 75 nm the mean Ti:Nb ratio is 0.51 ± 0.32. Only a few of the particles in the range from 25 to 20 nm were observed to contain V, which is somewhat surprising as the base plate contained 0.068 wt % V. However, as was the case for the 350 WT CAB steel, it is believed that the majority of the very small particles, 10 nm or smaller in diameter, were (V,Nb) rich.

4.2 3 and 6 kJ/mm Gleeble Samples

The size distribution of particles in the 3 and 6 kJ/mm Gleeble samples were similar to that found in the base plate, although there was a small but significant decrease in the mean particle size, 58 ± 30 nm for the 3 kJ/mm and 43 ± 21 nm for the 6 kJ/mm samples compared to 77 ± 37 nm in the base plate. Accompanying this change in mean particle size was an increase in the Ti/Nb ratio from 0.90 ± 0.31 in the base plate to 1.58 ± 0.61 after the 3 kJ/mm thermal cycle and 1.66 ± 0.45 after the 6 kJ/nm thermal cycle. It is thought that the principal reasons for this behaviour are again the loss of the Nb-rich "caps" on the Ti-rich cuboids and the formation of Ti-rich "skins" at the surface of the cuboids as they attempt to reach an equilibrium composition at the peak temperature of the Gleeble thermal cycle[3]. After the thermal cycles all the small (< 20 nm) spheroidal particles had dissolved and the remaining particles were faceted (Fig. 19).

4.3 3 and 6 kJ/mm Welds

The analysis of the composition of particles as a function of distance from the fusion line in the welds again proved to be a more sensitive way of monitoring the changes than following the mean particle size. Although there was a greater density of particles/grid area in this steel than in the other three steels studied, the numbers were still too low to obtain meaningful size data from a single replica. The composition

data as a funciton of distance for the 3 and 6 kJ/mm welds is shown in Fig. 20. As the fusion line is approached the Ti/Nb ratio increases. The maximum value found, Ti/Nb ~ 2.8, is less than the greatest value in the HAZ of the CAB treated steel, Ti/Nb ~ 5, but as we have already noted the mean value of the Ti/Nb ratio in the particles in the base plate of the ingot cast steel, 1.94 ± 0.57, was approximately double the value in the continuously cast steel, 0.90 ± 0.31.

In both welds a very narrow region of the HAZ next to the fusion line ~ 40-80μm wide, was devoid of any particles but within the area of the first grid a few particles could usually be found. All particles > 10 nm in size close to the fusion line in both welds had a faceted, cuboidal morphology, in agreement with the Gleeble thermal simulation results. Two examples are shown in Fig. 21; the first shows particles 10-30 nm in diameter in the 3 kJ/mm sample, ~ 0.1 mm from the fusion line; the second, taken from the same sample, ~0.5mm from the fusion line, contains a range of particle sizes. (The cluster of particles in Fig. 21 (b) is probably the transformed product of a single dendrite particle in the as-cast structure discussed earlier). There was also evidence in some areas of the 6 kJ/mm weld of reprecipitation effects e.g. Fig 22, which comes from an area ~ 0.7 mms from the fusion line in the bay region of the weld. Again we note the similarity to the observations made in the LT60 and 350 WT CAB steels at the same heat input.

5. References for Part A

1. G. Cliff and G.W. Lorimer, J. Microscopy, 103, 203 (1975)
2. D.C. Houghton, G.C. Weatherly and J.D. Embury, "Thermochemical Processing of Microalloyed Austenite", p.267, The Met. Soc. of A.I.M.E. (1981)
3. D.C. Houghton, G.C. Weatherly and J.D. Embury, "Advances in the Physical Metallurgy and Applications of Steels", p.136, Book 284, The Metals Society, London (1982)
4. S. Suzuki, G.C. Weatherly and D.C. Houghton, Acta metall, 35, 341 (1987)
5. R.C. Sharma, V.K. Lakshmanan and J.S. Kirkaldy, Met. Trans, 15A, 545 (1984)
6. H.B. Aaron and G.R. Kotler, Met. Trans, 2A, 393(1971)
7. B. Sparke, D.W. James and G.M. Leak, J. Iron Steel Inst., 203, 152 (1965)
8. V.K. Lakshmanan and J.S. Kirkaldy, Met. Trans, 15A, 541 (1984)
9. J.J. Jonas and M.G. Akben, Metals Forum, 4, 92 (1981)

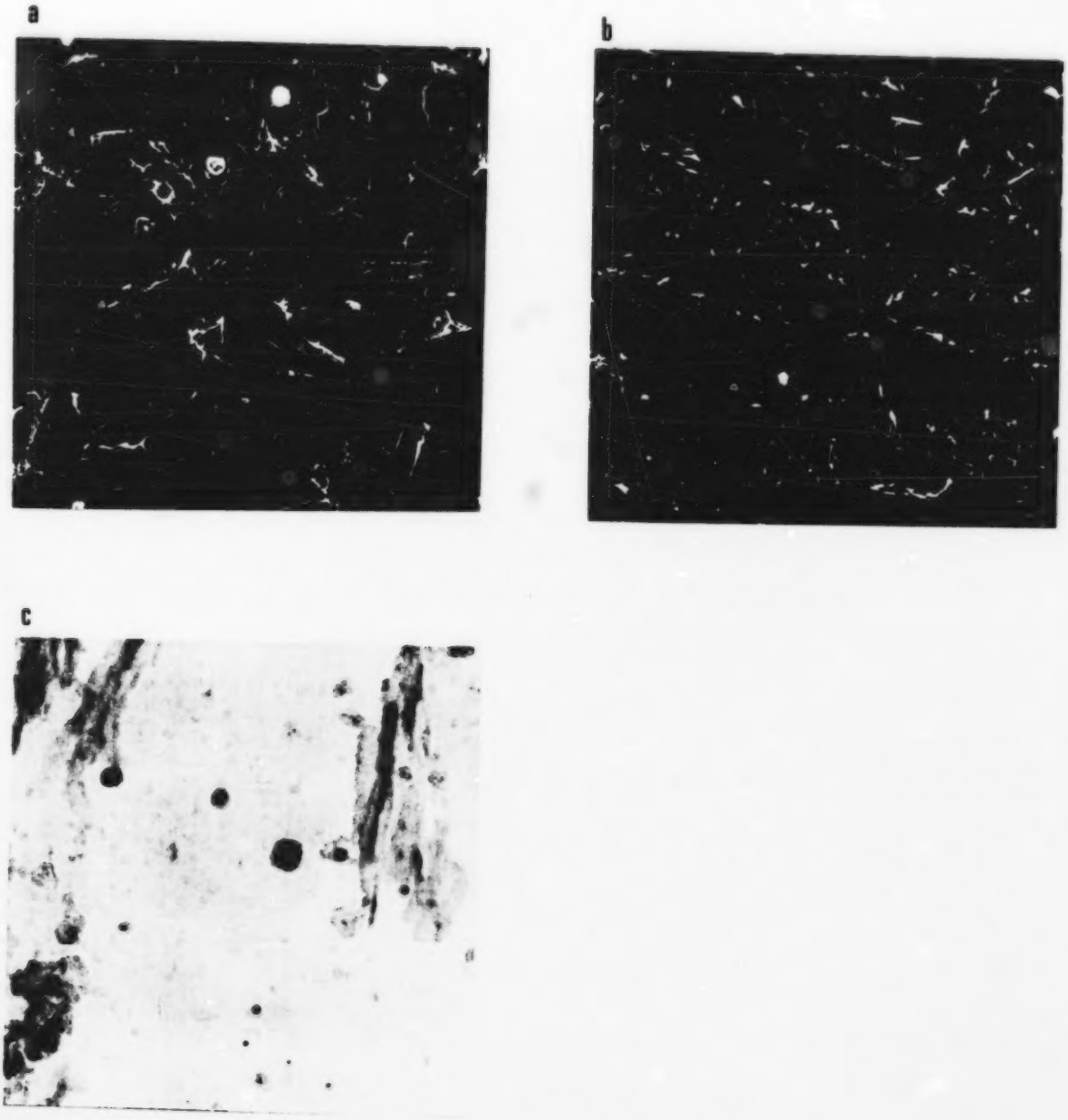

Figure 1 Replica of bay region of 3 kJ/mm weld of 4360D steel showing
(a) weld metal (x15000)
(b) fusion line region in adjacent grid to (a) (x15000), and
(c) precipitates 2mm from the fusion line (x60000)

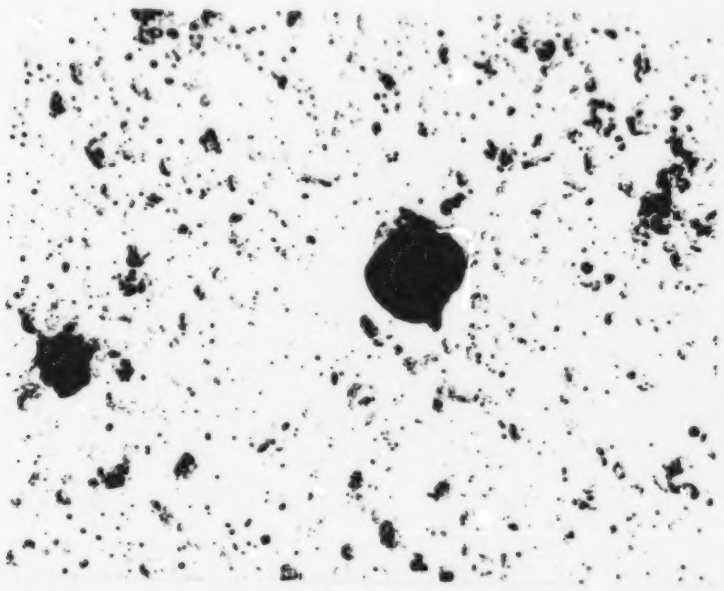

Figure 2 Bimodal distribution of coarse and fine Nb-containing particles in 4360D base plate (x60,000)

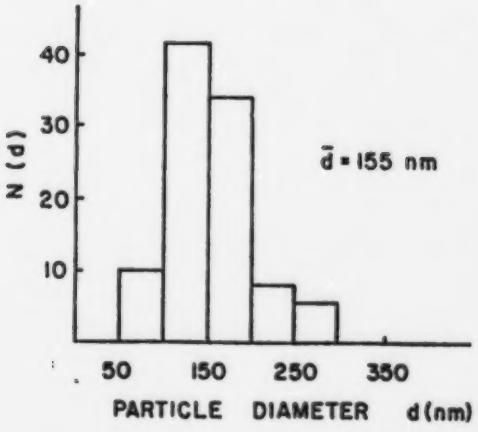

Figure 3 Size distribution of coarse particles, 50-300 nm in diameter, $\bar{d}$ = 155nm, in base-plate of 4360D steel

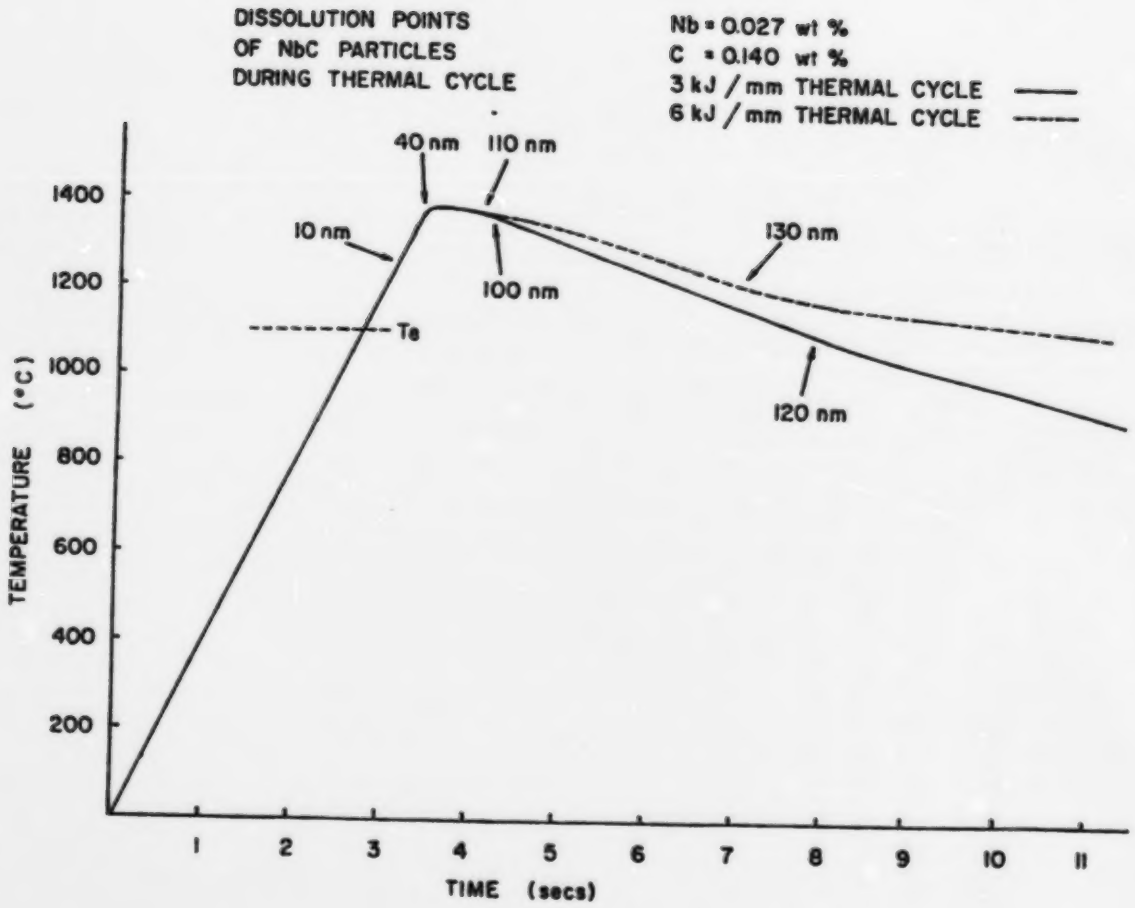

Figure 4 Calculated points of dissolution of NbC particles of varying size for the 3 and 6 kJ/mm thermal cycles. The steel was assumed to contain 0.027 wt % Nb and 0.14 wt % C

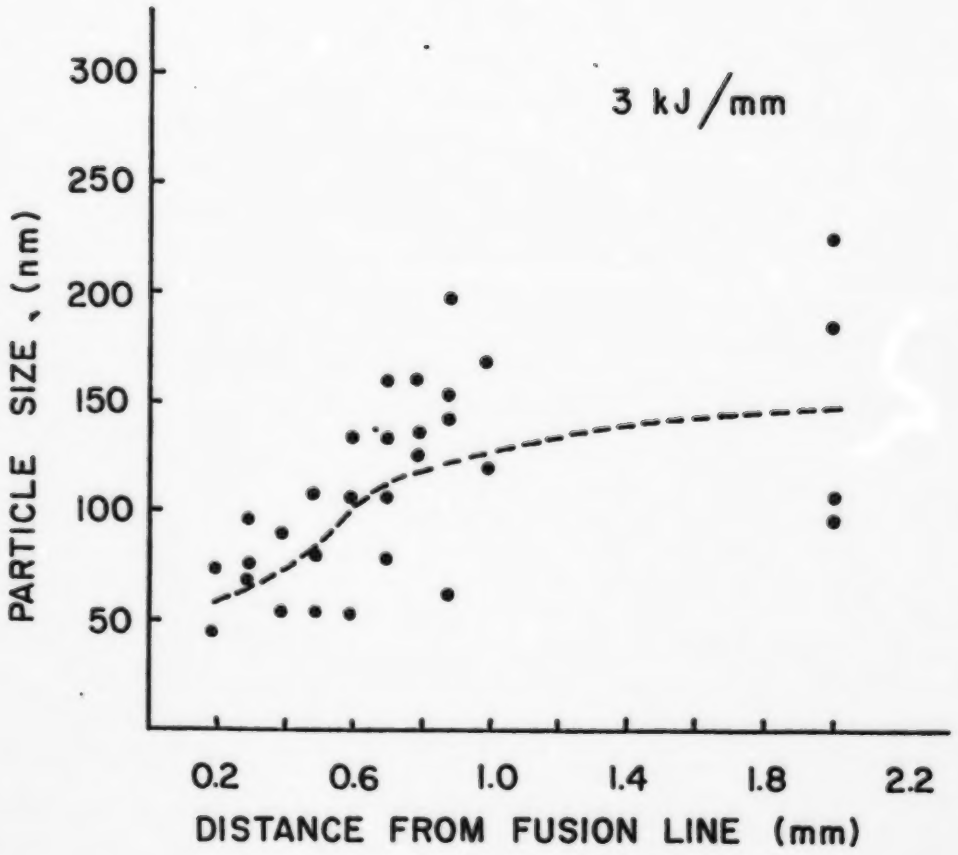

Figure 5 Distribution of coarse Nb(C,N) particles in the HAZ weld bay region of 4360D as a function of distance from the fusion line. The points represent individual readings taken in successive grid areas

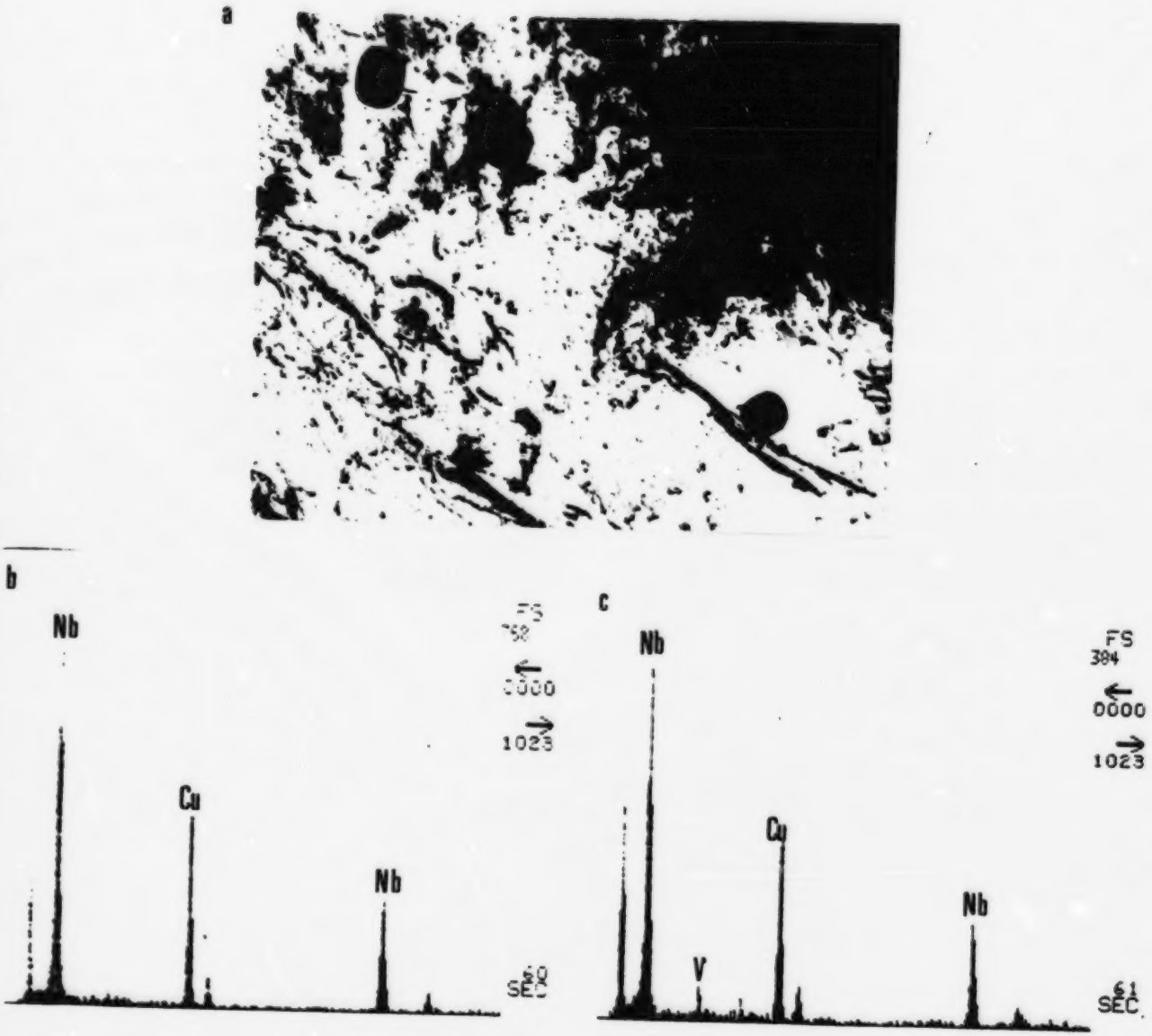

Figure 6 (a) Analysis of bimodal particle distribution found in LT60 steel (x30000)
(b) EDX spectrum from coarse particle showing only Nb
(c) EDX spectrum from finer particles showing both Nb and V peaks

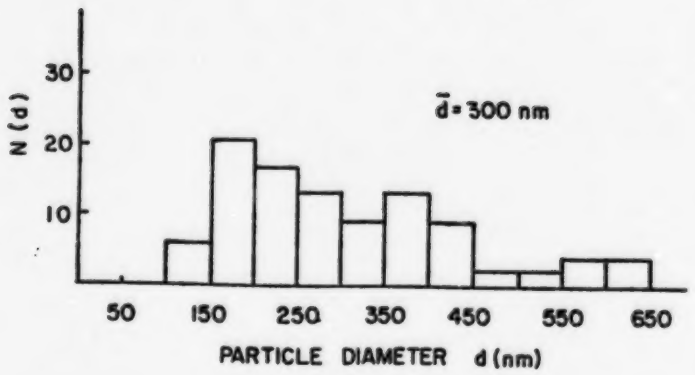

Figure 7 Size distribution of coarse Nb-rich particles, 125-600 nm in diameter, $\bar{d}$ = 300 nm, in base plate of LT60 steel

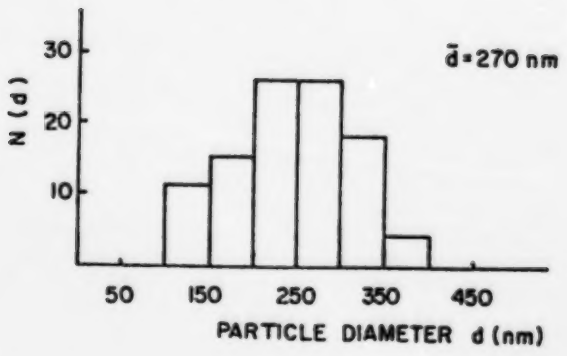

Figure 8 Size distribution of Nb-rich particles after 6 kJ/mm thermal cycle, 100-400 nm in diameter, $\bar{d}$ = 270 nm

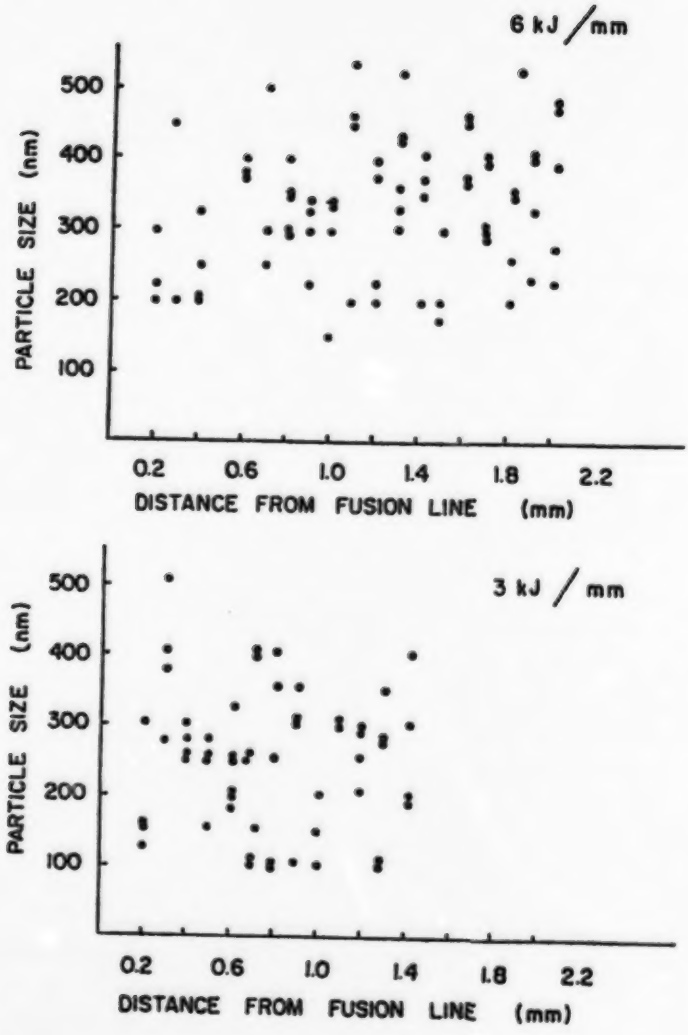

Figure 9 Distribution of coarse Nb(C,N) particles in the HAZ weld bay region of LT60 steel as a function of distance from the fusion line

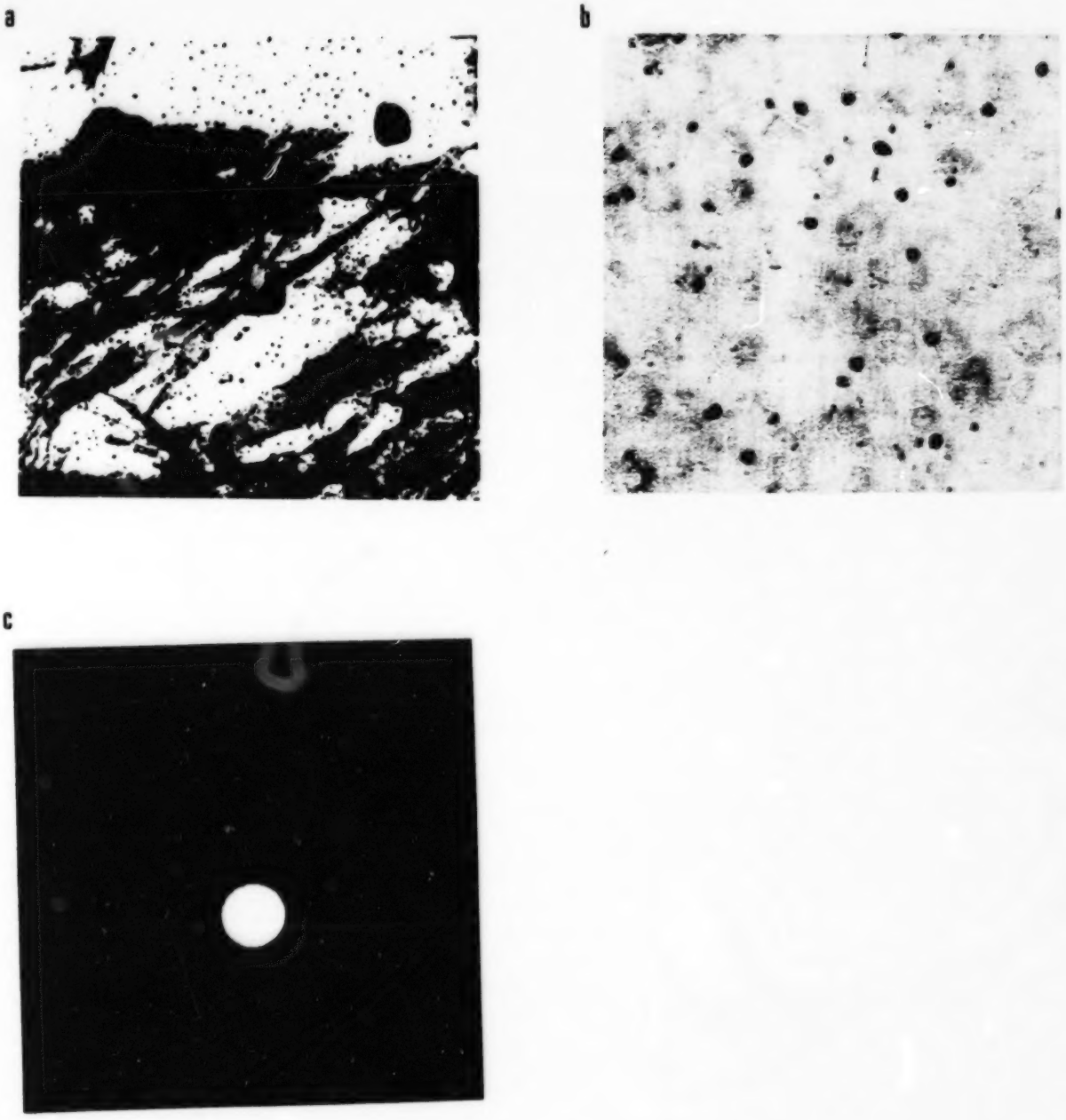

Figure 10 Fine scale precipitation observed in the bay region of LT60 HAZ at a heat input of 6 kJ/mm
(a) 0.2 mm from the fusion line (x30,000)
(b) at the fusion line (x150,000)
(c) diffraction pattern from area shown in (b)

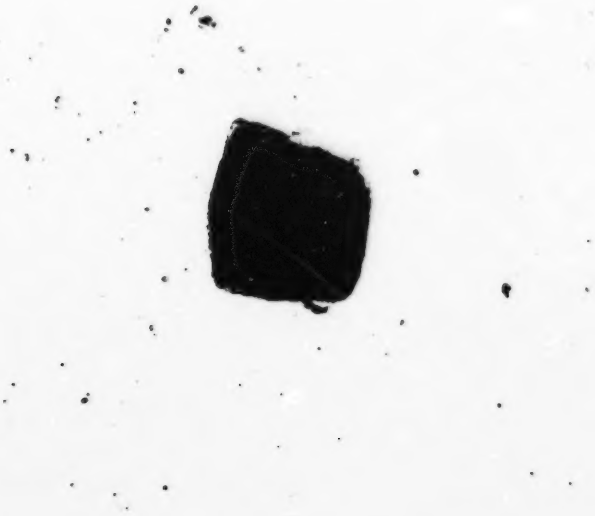

Figure 11 Bimodal distribution of coarse and fine precipitates in 350 WT CAB steel. Note cap on cuboidal particle (x150,000)

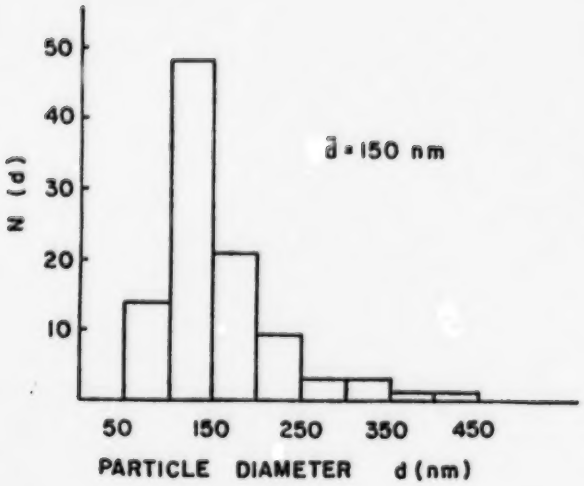

Figure 12 Size distribution of coarse particles, 50-450 nm in diameter, $\bar{d}$ = 150 nm, in base plate of 350 WT CAB steel

Figure 13 Microstructure of 350 WT CAB steel showing faceted particles and absence of fine scale precipitation after 6 kJ/mm Gleeble thermal cycle (x45,000)

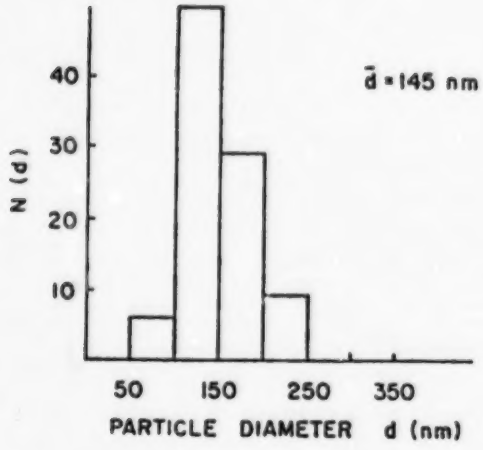

Figure 14 (a) Size distribution of coarse particles, 100-250 nm in diameter, $\bar{d}$ = 145 nm, in 350 WT CAB steel after 3 kJ/mm Gleeble cycle

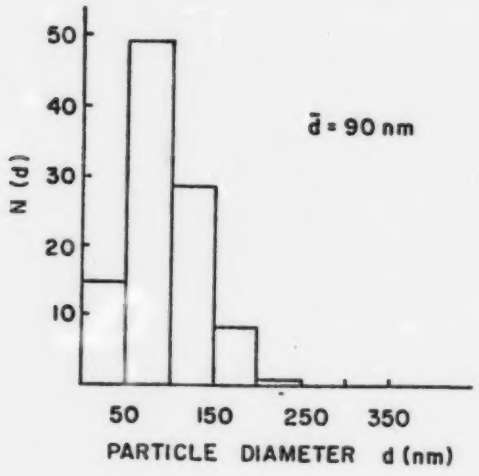

Figure 14 (b) As (a), after 6 kJ/mm Gleeble cycle, $\bar{d}$ = 90 nm

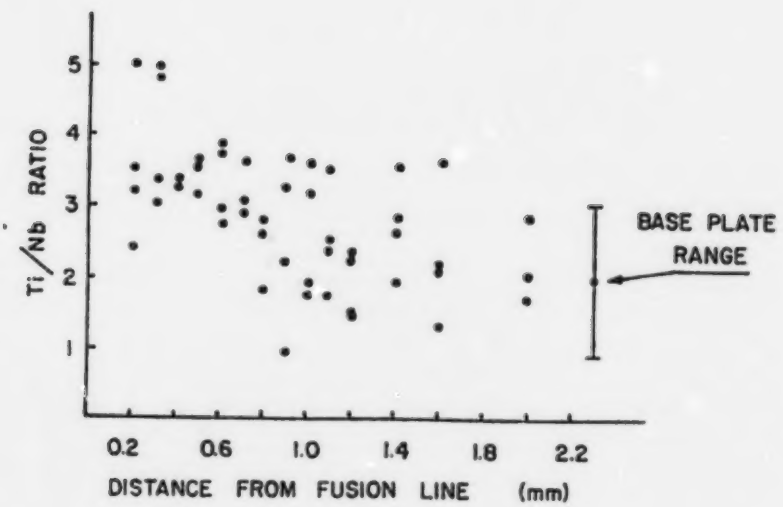

Figure 15 Variation of Ti/Nb weight ratio in coarse particles as a function of distance from the fusion line in 350 WT CAB steel weld (3 kJ/mm heat input)

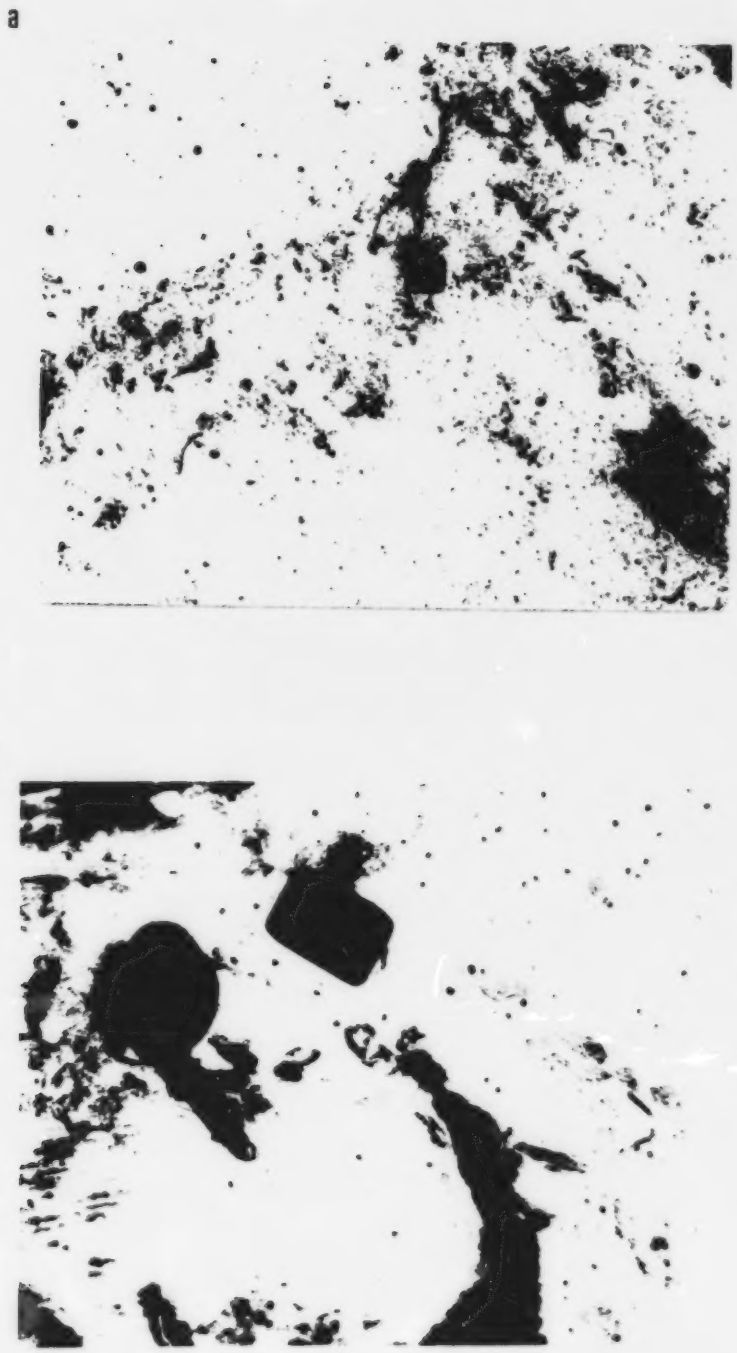

Figure 16 Fine scale precipitation in bay region of HAZ of welds from 350 WT CAB steel
(a) 3 kJ/mm, 0.4 mm from fusion line (x45,000)
(b) 6 kJ/mm, 0.3 mm from fusion line (x60,000)

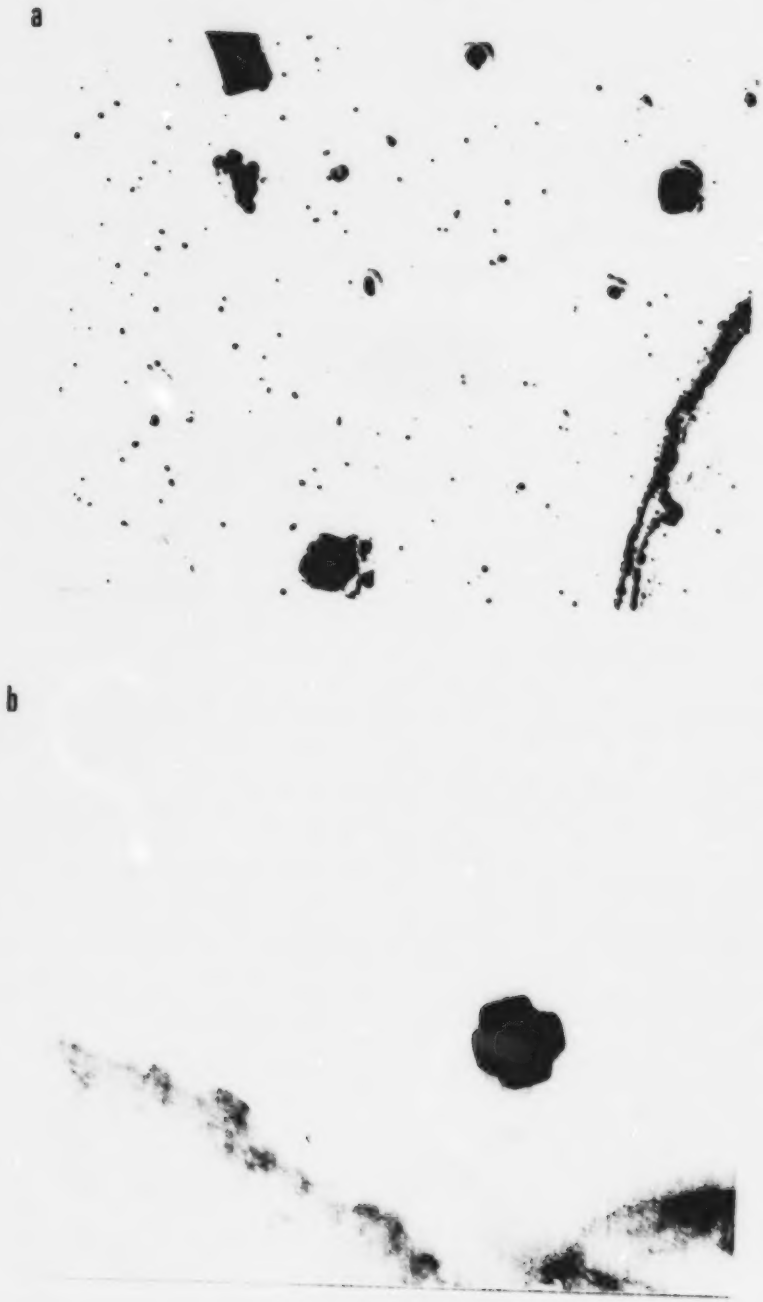

Figure 17 Distribution of particle morphologies and sizes in base plate microstructure of 350 WT STRAND CAST steel
(a) cuboidal and spheroidal (x90,000)
(b) faceted star-shaped (x60,000)

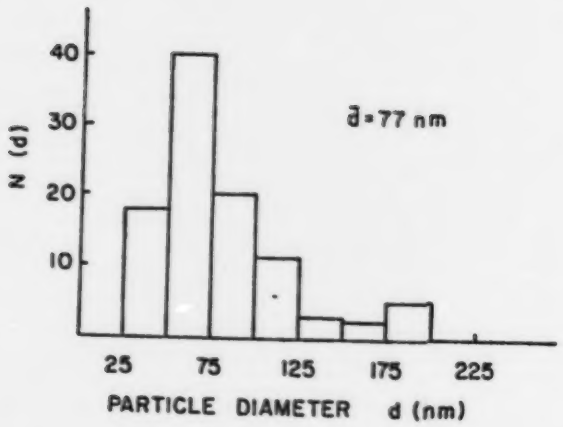

Figure 18 Size distribution of particles in 25-200 nm range, $\bar{d}$ = 77 nm, in base plate of 350 WT STRAND CAST steel.

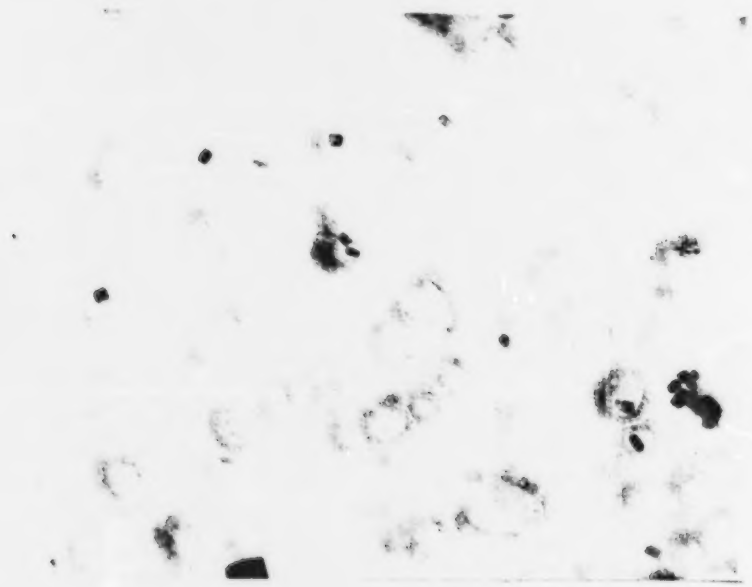

Figure 19 Small faceted particles in 6 kJ/mm Gleeble sample of 350 WT STRAND CAST steel (x90,000)

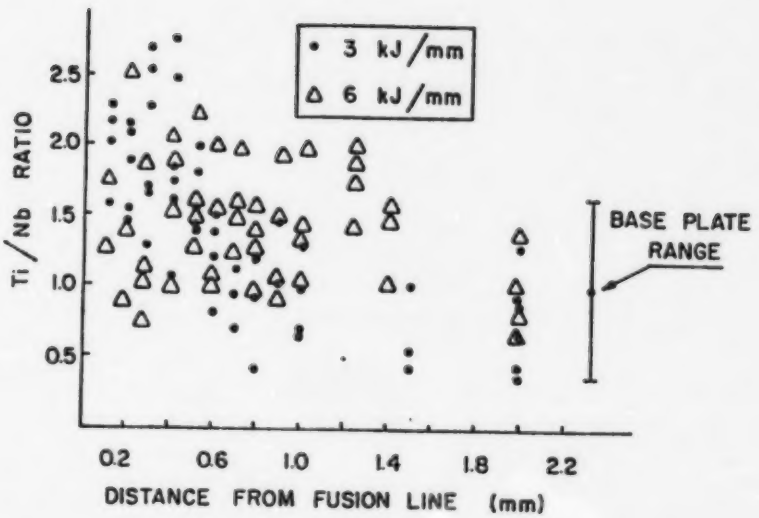

Figure 20 Variation of Ti/Nb weight ratio in particles as a function of distance from the fusion line in 350 WT STRAND CAST steel weld for 3 and 6 kJ/mm heat inputs

Figure 21 (a) Small faceted particles ~ 0.1 mm from the fusion line in 3kJ/mm weld of 350 WT STRAND steel (x150,000)

Figure 21 (b) Range of particle morphologies in same sample ~ 0.5 mm from the fusion line (x75,000)

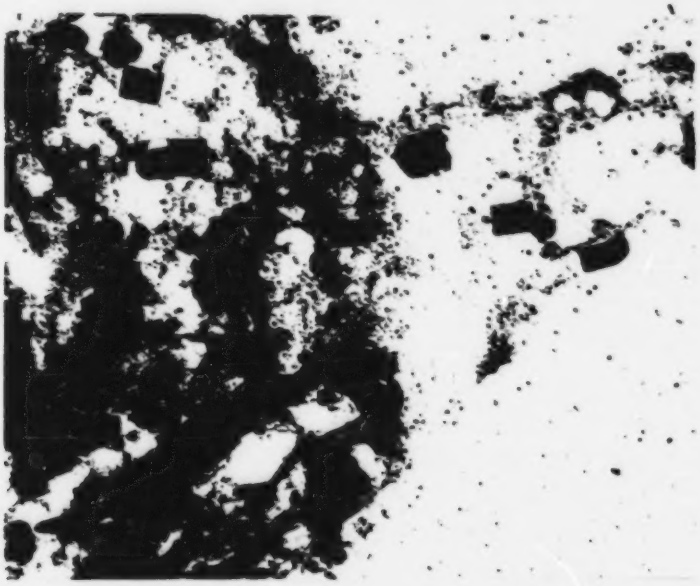

Figure 22 Fine scale precipitates in bay region of HAZ of weld, ~ 0.7mms from the fusion line, 350 WT Strand Cast Steel, 6 kJ/mm heat input (x60,000)

Part B Characterization and Identification of Microstructural Transformation Products

The phase transformation products associated with the decomposition of austenite were studied using scanning and transmission electron microscopy. Gleeble simulation samples with heat inputs corresponding to 3 or 6 kJ/mm were used; as before all the observations were taken from the centre line of the samples, where the peak temperature of 1375°C was reached during the simulations.

Standard metallographic preparation techniques were used for the samples to be studied by scanning electron microscopy. Samples were etched for 2 min in a solution of 4% picric acid in ethanol prior to examination. For transmission electron microscopy thin slices were carefully removed by spark machining from the centre region of the Gleeble samples and chemically polished to about 100 µm thickness. Three mm. discs were then cut from the thin sheet and electropolished in a solution of 16% perchloric acid, 64% ethanol, 9% butylcellusolve and 11% water at -25°C.

The range of samples studied and approximate prior austenite grain sizes (determined by optical metallography) are listed in Table 1.

Table 1

Samples Studied

Steel	Heat Input	Prior Austenite Grain Size
LT60	3kJ/mm	~ 200µm
LT60	6kJ/mm	~ 250µm
350 WT CAB	3kJ/mm	~ 180µm
350 WT CAB	6kJ/mm	~ 260µm
350 WT ST	3kJ/mm	~ 100µm
350 WT ST	6kJ/mm	N.A.*
4360 50D	6kJ/mm	~250µm

*Not Available. The prior austenite grain size could not be revealed by the polishing and etching procedures adopted in this study (see e.g. Fig. 6a)

Results

LT60

The microstructures of the LT60 sample after a thermal cycle corresponding to a heat input of 3kJ/mm are shown in Fig. 1. At low magnification (Fig. 1a the prior austenite grain boundaries are clearly visible, while at higher magnification (Fig 1b) the scanning electron micrograph shows a bainitic structure with litte or no evidence of pro-eutectoid ferrite. The bainitic microstructure consists of parallel laths of ferrite separated by low angle boundaries containing elongated plates of the M-A phase or carbides (Figs 1c, 1d). Both the S.E.M. (Fig. 1b) and T.E.M. micrographs (Fig. 1c) show that within a single colony of ferrite laths that comprises the basic structural 'unit' of the transformation product the interlath phase may be either the M-A phase or iron carbides. The M-A phase could be readily identified by the characteristic streaking in the diffraction patterns associated with the fine scale twinning in this phase (Fig. 1d).

At the higher heat input of 6kJ/mm, the microstructure showed regions of proeutectoid ferrite, formed at prior austenite grain boundaries (Fig. 2a) and some aligned ferrite, associated with MA or carbides, but there were also regions where intragranular blocky ferrite had formed (Fig. 2b). In these regions the retained MA phase or carbides had an 'island' morphology (Fig. 2b) rather than the elongated structure associated with the classical upper bainite morphology shown in Fig. 1.

350 WT CAB

The 3kJ/mm heat input thermal simulation for this steel gave a very similar microstructure to that found for the LT60 steel. Again the prior austenite grain boundaries were clearly visible at low magnification (Fig. 3a); at higher magnification (Fig. 3b) the ferrite lath structure of upper bainite was seen with the laths separated by elongated islands of the MA phase (Fig. 3c) or carbides (Figs 3d, 3e). In this particular example carbon extraction replicas were also used to identify the Fe-rich carbides lying at the sub-boundaries between the laths within an individual upper bainite packet. (Fig. 3e)

At the higher heat input, the microstructures were again almost identical to those found with LT 60. Pro-eutectoid ferrite at prior austenite grain boundaries (Fig. 4a) with regions of intragranular blocky ferrite and the more classical upper bainite structure were observed (Fig. 4b). The interlath phase in the upper bainite structure was predominantly a

carbide, but again regions containing both MA and carbides were found within a single bainite packet (Fig. 4b).

350 WT STRAND

For a heat input of 3kJ/mm, the dominant microstructure was again upper bainite, with little or proeutectoid ferrite at prior austenite grain boundaries (Fig. 5a). The phase found between the ferrite laths was usually the MA phase (Fig. 5b, 5c) but in some areas there was evidence of carbide formation (Fig. 5b) and the MA phase was also found as twinned islands in the ferrite matrix (Fig. 5d). In comparing the 350 WT strand-cast steel to the 350 WT CAB-treated and LT 60 steels at this heat input, the 350 WT ST steel had a greater proportion of the MA phase between the ferrite laths.

No prior austenite grain boundaries could be identified in the 350 WT ST steel at the higher heat imput and the microstructure appeared quite different from 350 WT CAB and LT 60. Although there were a few patches of an upper bainite aligned structure (Fig. 6a) most of the structure consisted of blocky grains of ferrite (roughly 10μm in size). The C-rich regions consisted either of islands of the MA phase or pearlite, although again there was proportionally more MA phase than in the 350 WT CAB and LT 60 steels at this heat input. (Fig. 6b).

4360 - 50D

This steel was only examined at the higher heat input of 6kJ/mm. The structure was similar to that found with the 350 WT CAB and LT 60 steels, viz. some proetutectoid ferrite at prior austenite grain boundaries (Fig. 7a) and a mixture of aligned and blocky ferrite (Fig. 7a, 7b). The phase between the ferrite laths and grains was predominantly a carbide (Fig. 7c).

Discussion

The results reported above for the four steels show the expected trends with heat input and composition. At a heat input of 3kJ/mm the dominant microstructure in all four steels was an aligned upper bainite with little or no proeutectoid formation at the prior austenite grain boundaries. As the heat input was increased to 6kJ/mm, proeutectoid formation was observed and the ferrite structure within the grains was a mixture of an aligned ferrite and equiaxed blocky ferrite.

The similarities noted in this study in the microstructures of the LT 60, 350 WT-CAB and 4360-50D steels and the marked difference between these three steels and the 350 WT-ST steel are related to the compositions of the base plate (see Table I in Part A) and the processing conditions used in the fabrication of the 350 WT-CAB and 350 WT-ST steels. The major differences between the steels are the lower carbon content of 350 WT-ST, (0.07 wt % versus 0.12-0.15 wt % for the other three steels) and the smaller grain size of 350 WT-ST, which is a consequence of the fine distribution of (Ti, Nb) (C, N) cuboids in the strand-cast steel (see Part A). Both these factors result in a much lower hardenability for the 350 WT-ST grade, so that at the higher heat input, the decomposition product during cooling is a blocky or grain-boundary nucleated ferrite rather than an aligned ferrite structure. On the other hand, the three other steels have similar compositions and prior austenite grain sizes and the microstructures of these steels are expected to be similar.

The nature of the C-rich phase formed during cooling can also be related to the base plate composition and cooling rate. Previous studies [1,2] have shown that at a fixed cooling rate, increasing the C content (while keeping the composition of all other elements approximately the same) promotes the formation of carbides rather than the M-A phase when bainite or acicular ferrite forms. Conversely at a fixed C content, increasing the heat input (equivalent to an increase in the $t_{800\text{-}500°C}$) promotes the formation of carbides rather than the MA phase[2]. This explains the trends noted in the experimental results:

(1) For a given steel increasing the heat input from 3 to 6 kJ/mm promotes the formation of carbides rather than MA associated with the ferrite laths.

(2) The proportion of MA phase is higher in 350 WT-ST (0.07 wt % C) than in the other three steels (0.12-0.15 wt % C) at the same heat input.

References

1. L.J. Habraken and M. Economoponlos, Symposium on "Transformation and Hardenability in Steels", Climax Molybdenum Company (1967)

2. A.G. Glover, J.T. McGrath, M.J. Tinkler and G.C. Weatherly, Welding J., Sept 1977, 267s (1977)

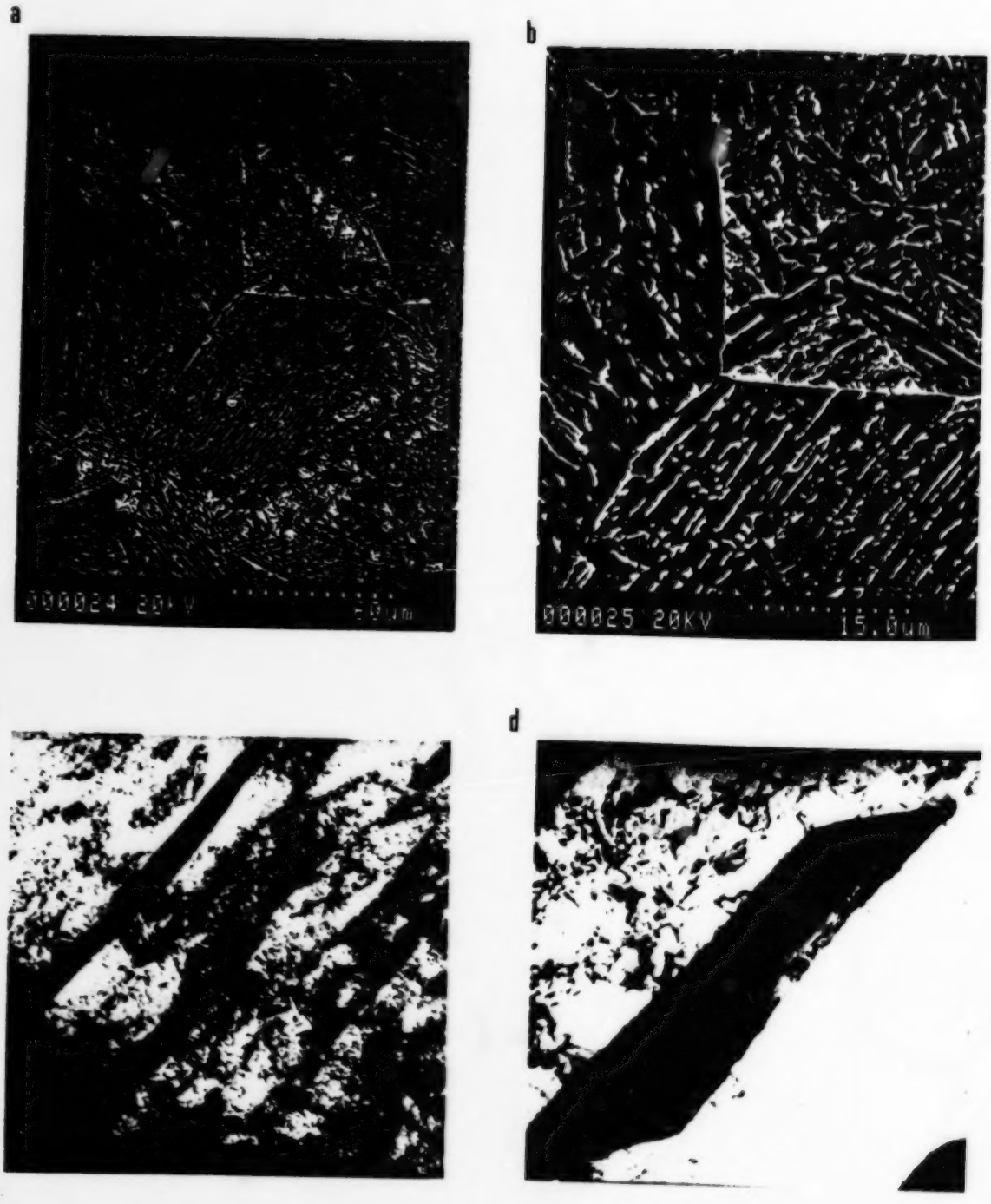

Fig. 1 Microstructures of LT60 subjected to 3kJ/mm thermal simulation a) SEM showing prior austenite grain boundaries and bainite structures b) as (a) higher magnification c) TEM thin foil elongated MA phase and carbides (x 12,000) d) TEM thin foil twinned marteniste in MA phase (x 30,000)

a

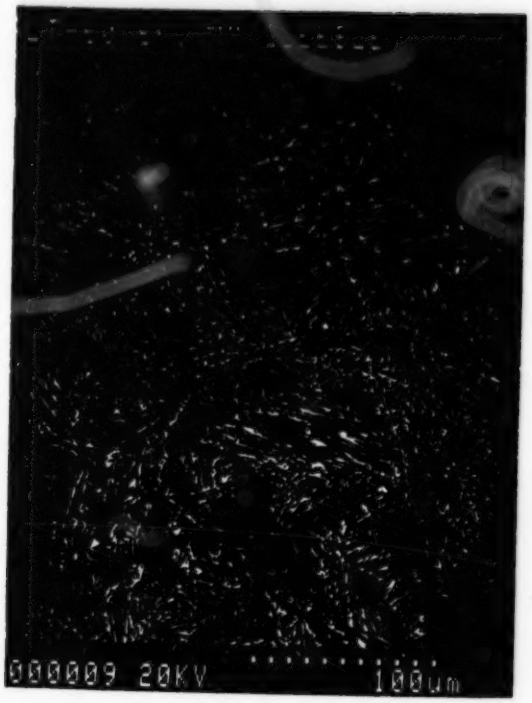

b

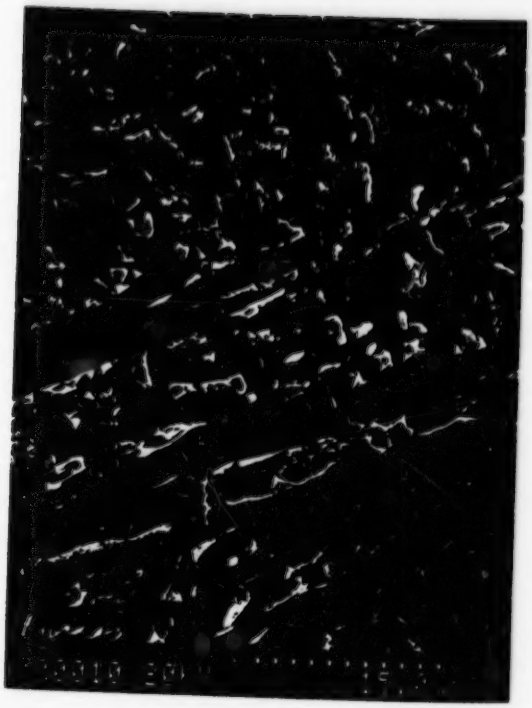

Fig. 2 S.E.M. microstructures of LT60 subjected to 6 kJ/mm thermal simulation

a) proeutectoid ferrite at prior austenite grain boundaries with aligned ferrite and blocky intragranular ferrite b) as (a) showing islands of the MA pahse and carbides.

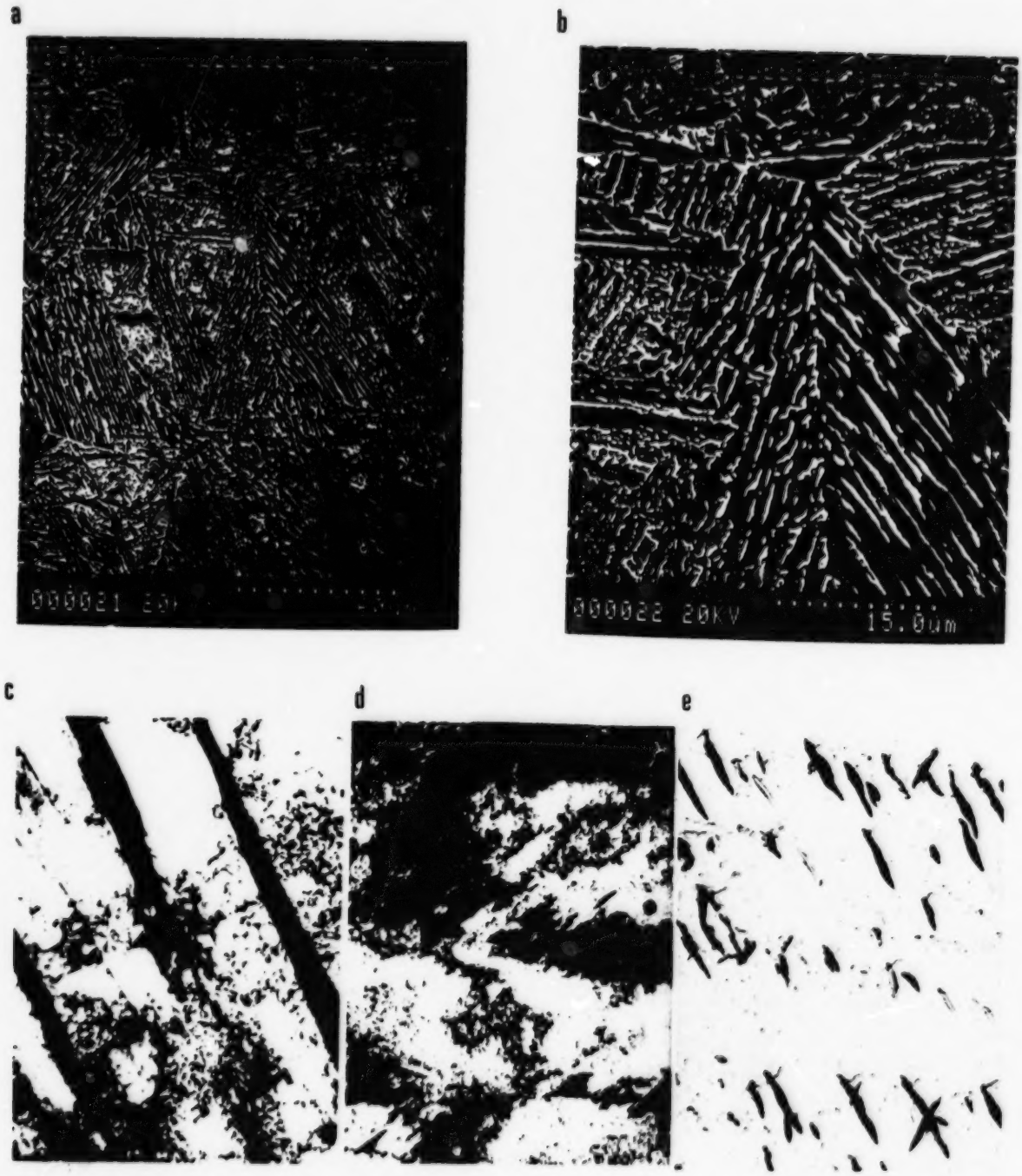

Fig. 3 Microstructures of 350WT-CAB subjected to 3kJ/mm thermal simulation a) SEM showing prior austenite grain boundries and bainite structures b) as (a) higher magnification c) TEM thin foil, aligned MA phase (x 30,000) d) TEM thin foil, carbides (x 10,000) e) extraction replica, carbides (x 20,000)

a

b

Fig. 4 S.E.M. microstructures of 350 WT-CAB subjected to 6kJ/mm thermal simulation

a) Proeutectoid ferrite at prior austenite grain boundries with aligned and blocky intragranular ferrite b) as (a) showing aligned rows of carbides between ferrite laths.

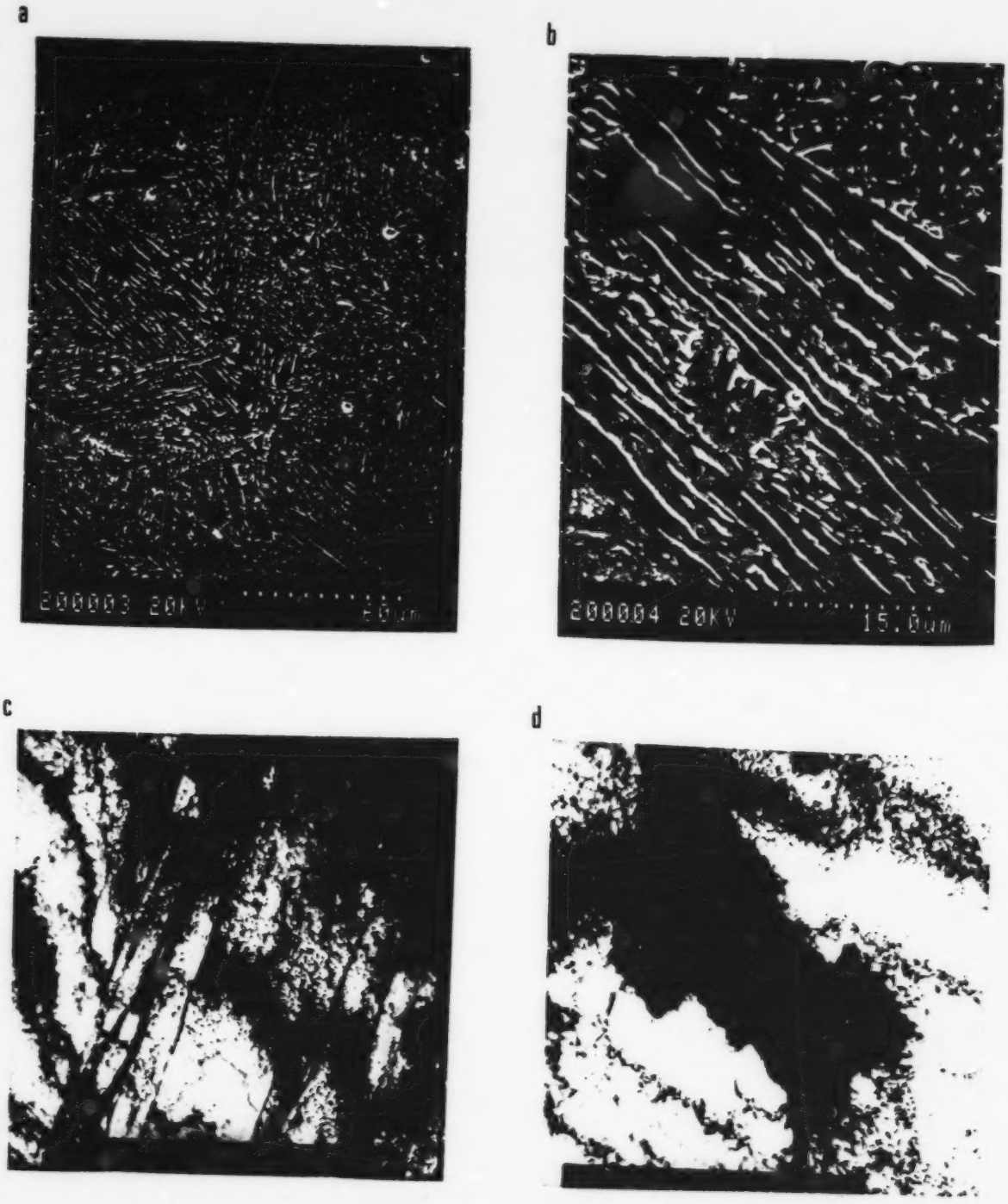

Fig. 5 Microstructures of 350WT-ST subjected to 3kJ/mm thermal simulation a) S.E.M. showing prior austenite grain boundaries and bainitic structures b) as (a) higher magnification, aligned MA phase c) TEM thin foil, aligned MA phase (x 12,000) d) TEM thin foil, island MA phase showing twins (x 20,000)

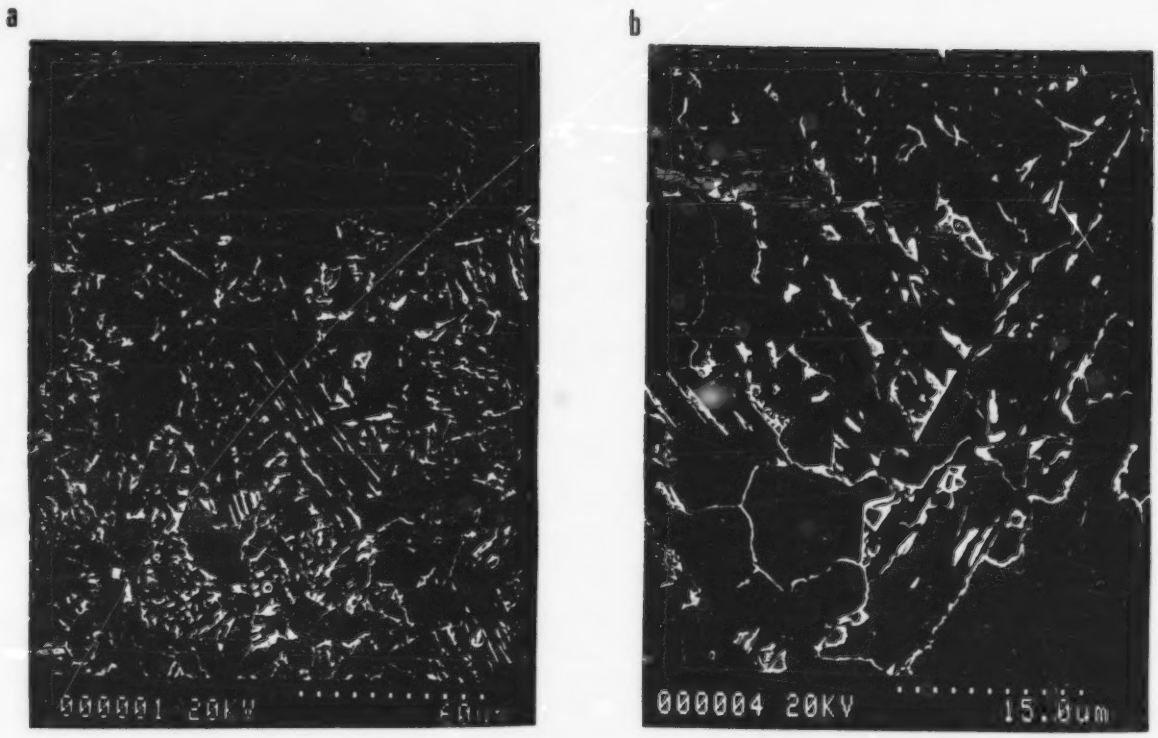

Fig. 6 S.E.M. microstructures of 350WT-ST, subjected to 6 kJ/mm thermal simulaiton

a) Blocky ferrite structure, b) as (a), higher magnification showing MA phase and carbide patches.

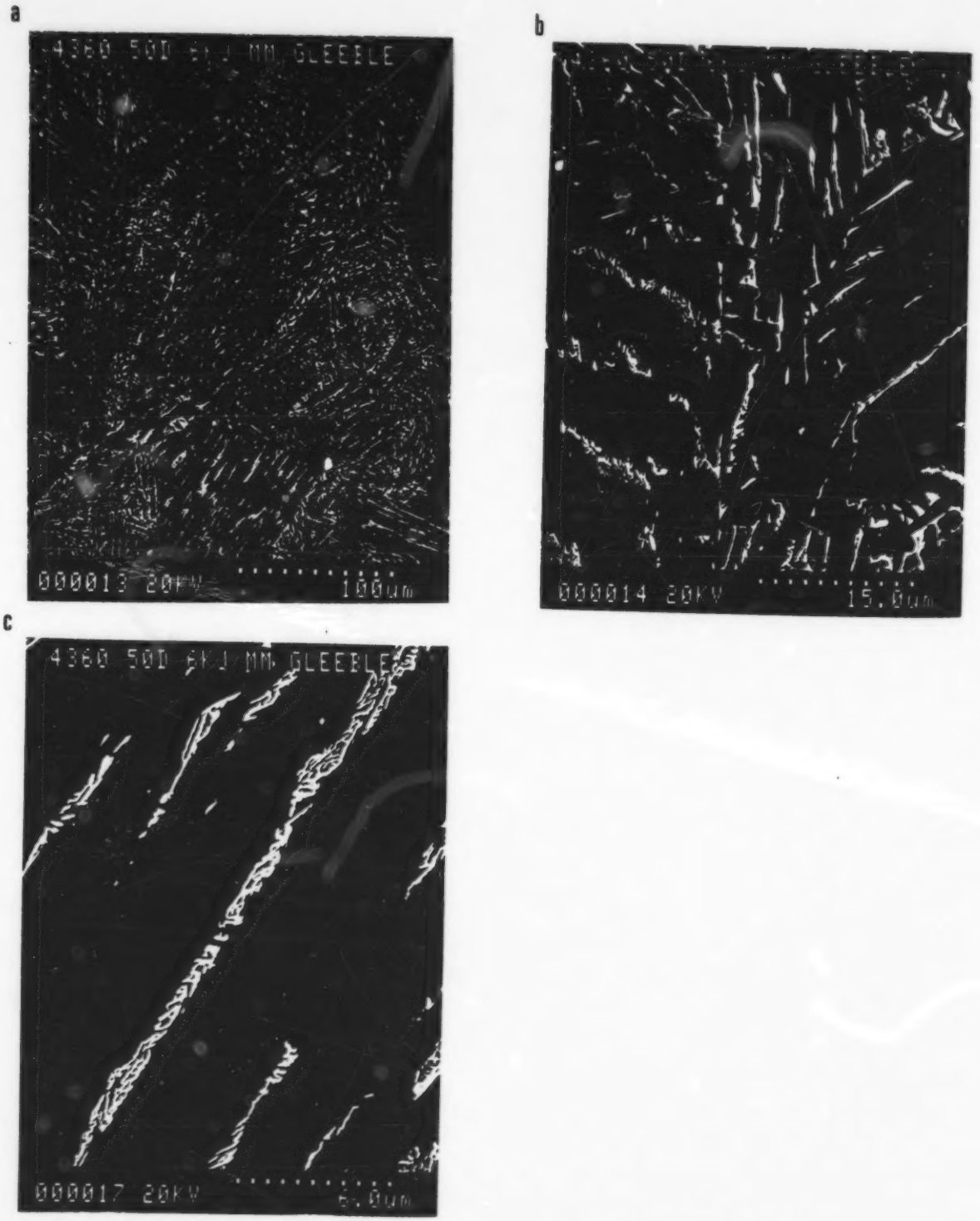

Fig. 7 SEM microstructures of 4360-50D, subjected to 6kJ/mm thermal simulation

a) Proeutectoid ferrite at prior austenite grain boundries with aligned and blocky intragranular ferrite

b) as (a), higher magnification showing aligned carbides c) as (b).

PART C CONCLUSIONS

1. Nb(C,N) particles in BS 4360D steel dissolve during the weld thermal cycle associated with 3 and 6 kJ/mm heat inputs. The rate of dissolution is in reasonable agreement with the predictions of a model based on diffusion controlled dissolution. By comparing the dissolution behaviour observed with Gleeble simulated samples (peak temp = 1375°C), it is suggested that in the actual weld samples a peak temperature of 1375° is reached close to the fusion line (< 0.3 mms) in the bay region of the welds.

2. The LT60 and BS4360D steels both contained a bimodal distribution of coarse and fine particles. In the Gleeble simulated samples the fine particles totally dissolve while the coarse particles partially dissolve (as described in 1). A higher fraction of particles survive the thermal cycle in the LT60 steel because of the larger mean particle size in this steel and its greater microalloy content.

3. Fine-scale precipitation is observed in the LT60 steel weldment at a heat input of 6 kJ/mm, while none was observed in the Gleeble sample at the same heat input. This was attributed to the slower cooling rate in the bay region of the weld and the possible nucleation role associated with deformation in the austenite due to relaxation of residual stresses in the HAZ of the weld. Both these factors would promote nucleation of particles during cooling in the welds.

4. The Ti and Nb-bearing 350 WT CAB treated steel also contained a bimodal distribution of precipitates : Ti-rich cuboidal particles with a mean diameter of 150 nm, Ti/Nb = 1.94 ± 0.57 and a distribution of much finer (Nb, V) containing particles, less than 20 nm in size. After Gleeble thermal cycling only minor changes were observed in the distribution of the coarse particles, but their mean composition had increased to 2.50 ± 0.97 (after 3 kJ/mm) and 3.10 ± 1.13 (after 6 kJ/mm). These changes were attributed to the loss of Nb-rich caps on the cuboids and the formation of Ti-rich "skins" at the surface of the cuboids.

5. The data obtained from particles in the weld HAZ region of the 350 WT CAB steels followed the same trends observed in the Gleeble simulated samples. An increase in the Ti/Nb content is found as the fusion line is approached. Again one significant difference was noted in the welds and Gleeble samples at both heat inputs - fine scale precipitation throughout the HAZ which is believed to occur on cooling.

6. The 350 WT strand cost steel contained a finer distribution of cuboidal particles, but they had a lower Ti content than the 350 WT CAB treated steel ($\bar{d}$ = 77 nm, Ti/Nb = 0.90 ± 0.31 compared to $\bar{d}$ = 150 nm, Ti/Nb = 1.94 ± 0.57). These differences were ascribed to the casting practise used to produce the two steels - continuous casting versus ingot casting. In addition to cuboidal or rounded cuboidal particles in the base plate a fine distribution of (Nb, V) rich spheroidal particles was observed.

7. The Gleeble simulated samples showed an increase in the Ti/Nb ratio in the coarse particles to 1.58 ± 0.61 (after 3 kJ/mm) and 1.66 ± 0.45 (after 6 kJ/mm) for the same reasons noted in conclusion (4) above. The weld HAZ regions showed the same trend of increasing Ti/Nb ratio in the particles as the fusion line was approached and evidence of fine-scale reprecipitation effects at the higher heat input.

8. All welds showed a narrow region, ~ 0.1 mm wide, devoid of all coarse particles, adjacent to the fusion line of the weld.

9. The transformation products of the CGHAZ were observed to be proeutectoid or blocky ferrite, upper and lower bainite with the interlath regions being either the MA phase or carbides. An increase in the C content of the base plate favoured the formation of carbides rather than the MA phase (at a given heat input), while an increase in the cooling rate (lower, rather than higher heat inputs) favoured the formation of the MA phase.